LA-UR- 09-06274

Approved for public release; distribution is unlimited.

Title:	PHELIX
Author(s):	C. L. Rousculp (X-1-PTA) P. J. Turchi (P-DO) W. A. Reass (AOT-RFE) D. M. Oro (P-23) J. R. Griego (MST-7) R. E. Reinovsky (X-DO) B. C. Cox (NSTec-LAO)
Intended for:	IEEE Transactions on Plasma Science

Los Alamos
NATIONAL LABORATORY
EST. 1943

Form 836 (7/06)

PHELIX

C. L. Rousculp, P. J. Turchi *Member, IEEE*, W. A. Reass, D. M. Oro, J. R. Griego, R. E. Reinovsky *Member, IEEE*, B. C. Cox

***Abstract*—The Precision, High-Energy density, Liner Implosion eXperiment (PHELIX) pulsed power driver is currently under development at Los Alamos National Laboratory. When operational PHELIX will provide 0.5-1.0 MJ of capacitively stored energy into cm size liners that will reach implosion velocities of 1-4 km/s with approximately 10-20 μs implosion time. Peak load currents will be in the 5-10 MAmp range. To do this the machine will employ a reusable, multi-turn primary, single-turn secondary transformer to couple the 100-120 kV Marx capacitor system to the load. The transformer has been designed toward a coupling coefficient of 0.9.**

PHELIX is designed to be portable with only an 8 x 25 ft^2 footprint. This will allow the machine to be taken to the experiment designer's diagnostic of choice. The first such diagnostic will the LANL proton-radiography facility. There the multi-frame, high-resolution, imaging capability will be used to study hydrodynamic and material phenomena

Crucial to the performance of PHELIX is a multi-turn primary, single-turn secondary, current step-up toroidal transformer, $R_{major} \sim 30$ cm, $R_{minor} \sim 10$ cm. The transformer lifetime should exceed 100 shots. Therefore it is essential that the design be robust enough to survive the magnetic stresses produced by high currents. In order to evaluate our design, two methods have been utilized. First, an analytical evaluation has been performed. By identifying the magnetic forces as $J_1^2/2\ \nabla L_1 + J_1 J_2 \nabla M_{12}$, where J_1 and J_2 are currents in two circuits, coupled by mutual inductance M_{12} and L_1 is the self-inductance of the circuit carrying current J_1, analytical estimates of stress can be obtained. These results are then compared to a computational MHD model of the same system and to a full finite-element, electromagnetic simulation.

***Index Terms*—Hydrodynamics, Proton Radiography, Pulse Power Systems, Transformer Coupling,**

I. Introduction

MaRIE (Matter and Radiation in Extremes) is Los Alamos National Laboratory's next-generation, conceptual signature facility [1]. MaRIE will build on LANL's core capability in materials science. Here the term extreme doesn't have to mean the very hottest or most dense conditions. Extreme can also mean the bifurcation points in a parameter, which lead to dramatically different dynamics of a system. For example, the phenomena of spall damage of a material occurs when two reflected shock waves combine to put a ductile material into extreme tension and cause the material to tear apart. Over a very small range of shock strengths there can be a range behavior. For low shock pressure, no observable damage occurs. Just below the spall damage threshold, incipient spall takes place where only void formation is observed. Finally, above the damage threshold, full spall occurs where the material is completely ripped in two. In **Fig. 1** the dynamic spall of a cylindrical metal coupon is observed.

MaRIE aims to bridge the "micron-gap" in material science diagnostics. At the submicron spatial scale there is scattering diagnostics which image crystal structure. This is the domain of defect consequences and microstructure interactions that drive material strength and damage evolution. On the super-micron scale there is imaging diagnostics either with x-rays or protons. The major goal of MaRIE is merge these regimes and transition from mere observation and validation to prediction and control of material properties. This truly represents an experimental and theoretical frontier in science.

The PHELIX project is aligned with the long-term goals of MaRIE. It will furnish a dial-able, and reproducible drive for continuum size material samples. Also, magnetically driven cylindrical liners have shown to have high azimuthal precision (< 50 μm for cm size liners). The fundamental cylindrical geometry of liners has the property of being a converging while still admitting diagnostic access in the axial direction.

PHELIX is to be fielded within the existing LANL proton radiography facility [2]. Proton radiography offers the potential of 70 μm spatial resolution with 10-20 images over a few microsecond time interval. This higher spatial diagnostic resolution means that the experiment can be scaled down in size [3]. This means that less energy is needed from the driver, which means a less costly capital investment. The higher frame rate means that fewer shots need to be conducted in an experimental series, which translates into more economical science. Fig. 2. shows a conceptual picture of how a liner on target experiment would utilize proton radiography.

The notion of performing electromagnetically-driven, high energy-density hydrodynamic implosion experiments at greatly reduced total energy was introduced in a concept called PHELIX (Precision, High Energy-Density, Liner Implosion experiment) [4]. The impetus for this approach was the recognition that precision diagnostic techniques, such as proton radiography, could usefully examine implosions at cm and mm scales that would not require

Manuscript received September 30, 2009. This work was supported by the U.S. Department of Energy under Contract No. DE-AC52-06NA25396.

C. L. Rousculp is with Los Alamos National Laboratory, PO Box 1663, Los Alamos, NM, 87545 USA (phone: 505-665-3678, email: rousculp@lanl.gov) s

application of multi-megajoule capacitor banks (e.g., Atlas). The costs and difficulties of building and operating such banks can preclude pursuit of pulsed power techniques for important hydrodynamic studies. The more modest inductance change associated with smaller implosions, however, demands that we employ transformer circuitry in driving the liner. Such circuitry can involve complex electromagnetic forces, the analysis of which we discuss here.

II. PHELIX THE MACHINE

The PHELIX machine is designed to be portable and modular [2]. The general specifications are as follows:

- 4 Module – Single stage marx
- 120 kV air operation
- ATLAS rail gap switches
- $U_c \sim 0.5$ -1.0 MJ
- $I_{pk} \sim 5$ -10 MA
- B ~ 0.1 1.0 MG
- $T_{rise} \sim 2$ -5 μs
- 8 ft x 25 ft footprint
- $R_{linc} \sim 3$ cm
- $V_{liner} \sim 1$-4 km/s
- Air core toroidal transfomer coupling

Fig. 3 shows the PHELIX machine with the major features, including the vertically oriented transformer and experimental cassette.

The front and back view of a two marx assembly rack (240kJ) is shown in Fig. 4-5. The fiberglass support structure allows reliable 120 kV marx operation in air. Consideration of corona and surface tracking issues has been maintained to assure operations at the Los Alamos 7,600 feet altitude. This air insulation technique was proven with the ATLAS machine marx development. Testing with 50,000 shots resulted in only 2 railgap flash-guard failures. The structure must also accommodate the 600 lbs of each capacitor as well as rigging / lifting assemblies for fitting to the P-rad PHELIX trolley. The output header assembly includes "plate" damping resistors made of reticulated vitreous carbon foam [5]. These Los Alamos designed resistors are capable of 15 kA/cm2 with a dissipation of 120 J/CC. Each capacitor has a damping resistor able to mitigate system short circuits. The output cables are then used to directly wind the PHELIX transformer.

Once development and testing is complete, the system will be reconfigured onto the transportable PHELIX P-rad trolley asse

The major feature of the PHELIX machine is the current step-up transformer. This allows for modest size energy storage in the capacitor bank while still providing multi MAmps of current to the liner. Fig. 6 shows an exploded view of the components of the transformer.

The primary windings of the transformer are formed by 40, RG217 coaxial cables that deliver current from the capacitor bank. Pairs of cables are inserted into 20 segment pieces. These segments facilitate assembly of the transformer. The outer braid conductor of the cables is stripped back and connects to the segment. The inner conductor and insulator are internally wound 4 times around a plastic core. The cores have helical channels to support the cables. They are constructed via a 3D printing technology. Finally, the inner cable conductor is terminated on the segment via an exit hole.

The aforementioned segments and a single bottom plate form the single-turn secondary winding of the transformer. The bottom plate and single top plate form a short, narrow, low inductance (< 1 nH) transmission line to the cassette load. The top and bottom plates are held together by a series of post-hole bolts, which are insulated with top-hats and stand-offs.

The minor radius of the torus ($R_{minor} \sim 12$ cm) is chosen so as to achieve a primary to secondary winding coupling efficiency of 90% (k = 0.9). The major radius of the torus ($R_{major} \sim 36$ cm) is chosen based on R_{minor} and a close-packed spacing of the primary windings on the inside of the torus.

III. MODELING

Two modeling efforts have been undertaken. First, overall machine performance is analyzed with respect to circuit parameters as well as liner trajectory and velocity. Second, an effort to understand both the electrical performance as well as the mechanical integrity of the toroidal transformer is undertaken by both theoretical

A. Machine Performance Analysis

A lumped element circuit model has been constructed for use with the RAVEN 1D MHD code [5]. RAVEN solves the circuit equations along with the MHD for an experimental liner and target. Shown in Fig. 7 is a diagram of the circuit. Here C = 68 μF and 50 kV < V_0 < 100 kV are the capacitance and initial voltage on the bank. R_p = 20 mΩ and R_s = 0.1 mΩ are the accumulated internal resistances of the primary and secondary sides of the transformer. It should be noted that R_p consists primarily of a damping resistance to prevent voltage reversal of the capacitors. R = 10^9 Ω is an isolation resistor for modeling purposes. L_0 = 1 nH and L_1 = 34 nH are the net uncoupled inductances. These include cables inductances, capacitor and switch space inductance, and transmission line inductance. L_p = 395 nH and L_s = 24 nH are the coupled inductances of the toroidal transformer. The mutual inductance which couples the circuit loops is given by $L_m = k (L_p L_s)^{1/2}$. In RAVEN, the MHD load is implemented as a time-varying inductance and resistance for the circuit. The circuit provides a time-varying current (here I_s) that specifies a magnetic field boundary condition for the MHD.

Solution of the circuit equations and the MHD can proceed by specifying a simple liner and return conductor geometry. A liner cassette is shown in Fig. 8. The nominal dimensions are 2 cm axial length, 2.5 cm initial radius, 0.1

cm liner thickness, 0.1 cm gap between the liner and return conductor, and 0.5 cm thick return conductor.

Fig. 9 shows the RAVEN solution of the system. In Fig. 9(a), the current profiles for the primary and secondary windings of the transformer are shown. These correspond to I_p and I_s in Fig. 5. I_s is 180° out of phase with I_p and is approximately a factor of 4 greater in magnitude as is expected from a current step-up transformer. Rise time is slightly longer than 2 μs.

In Fig. 9(b) the voltage on the capacitor is shown. A value of 90 kV is the initial charge. Due to the 20 mΩ damping resistor, the voltage reversal is limited to < 30% to prevent damage to the bank.

In Fig. 9(c) the trajectories for the surface of the liner and return conductor are shown. RAVEN is a Lagrangian code, so that this amounts to tracking a given element over the duration of the calculation. The liner is driven radially inward and the return conductor radially outward under the jxB force of current running through their surfaces. Owing to its greater thickness, the inertia of return conductor moves more slowly than the liner.

In Fig. 9(d) the corresponding surface velocities of the liner and return conductor are shown. The liner accelerates to ~ 1 km/s in ~ 3 μs, while the return conductor reaches a speed of ~ 0.2 km/s. Though not shown here, over the course of the implosion, the Joule heating only melts the outer 10% of the liner. The integrity of the liner is especially important if it is to be used as a driver to shock a central target for damage type experiments.

B. Toroidal Transformer Stresses

We can use the inductance-gradient method to estimate forces and stresses in the PHELIX transformer. The general formula for the force on circuit '1' due to its current J_1 and to current J_2 in circuit '2' is [6]:

$$\mathbf{F}_1 = (J_1^2/2)\,\nabla L_1 + J_1 J_2\,\nabla M_{12} \tag{1}$$

Where L_1 is the self-inductance of circuit '1' and M_{12} is the mutual inductance between the two circuits. The gradient operators are taken in the direction of the change in magnitude of each geometric parameter that occurs in the expressions for self and mutual inductance. For example, if the self-inductance of a solenoid with N_1 turns is:

$$L_1 = \mu\pi N_1^2\, r_1^2/h \tag{2}$$

then the gradient would be:

$$\nabla = \mathbf{r}\,\partial/\partial r_1 + \mathbf{k}\,\partial/\partial h \tag{3}$$

where **r** and **k** are unit vectors in the radial (r_1) and axial (h) directions, respectively. The forces in the radial and axial directions are then:

$$F_r = \mu\pi N_1^2\, J_1^2\, (r_1/h) \tag{4a}$$

and

$$F_z = -\,\mu\pi N_1^2\, J_1^2\, (r_1/h)^2/2 \tag{4b}$$

Under the action of its own current, the coil tries to blow apart radially and squeeze axially.

For the PHELIX transformer, we essentially have a multi-turn solenoid inside a single-turn solenoid, with negligible fringing field because the field-lines are all contained within the solenoids, (thereby corresponding to the idealized situation to which Eqn. 2 applies). In this case, the coil "length" h is the circumference $2\pi R$ of the magnetic field-line that threads the common centers of the cross-sections of the primary and secondary coils. The self-inductances for the primary and secondary, respectively, are:

$$L_p = \mu N_p^2\, r_p^2/2R \tag{5a}$$

$$L_s = \mu N_s^2\, r_s^2/2R \tag{5b}$$

The mutual inductance is:

$$\begin{aligned} M_{ps} &= (\mu N_p J_p/2\pi R) N_s p r_p^2/J_p \\ &= (\mu N_s J_s/2\pi R) N_p p r_p^2/J_s \\ &= \mu N_p N_s r_p^2/2R \end{aligned} \tag{6}$$

The forces on each coil due their own currents are then:

$$F_{rpo} = \mu N_p^2 J_p^2\, (r_p/2R) \tag{7a}$$

$$F_{Rpo} = -\,\mu N_p^2 J_p^2\, (r_p/R)^2/4 \tag{7b}$$

and

$$F_{rso} = \mu N_s^2 J_s^2\, (r_s/2R) \tag{8a}$$

$$F_{Rso} = -\,\mu N_s^2 J_s^2\, (r_s/R)^2/4 \tag{8b}$$

The forces due to the coupling between the two coils are:

$$F_{rpm} = \mu N_p N_s J_p J_s r_p/R \tag{9a}$$

$$F_{Rpm} = -\,\mu N_p N_s J_p J_s r_p^2/2R^2 \tag{9b}$$

and

$$F_{rsm} = 0 \tag{10a}$$

$$F_{Rsm} = -\,\mu N_p N_s J_p J_s r_p^2/2R^2 \tag{10b}$$

The total forces on the coils in their respective minor and major radii are then:

$$F_{rp} = \mu N_p^2 J_p^2\, (r_p/2R) + m N_p N_s J_p J_s r_p/R \tag{11a}$$

$$F_{Rp} = -\,\mu N_p^2 J_p^2\, (r_p/R)^2/4 - m N_p N_s J_p J_s r_p^2/2R^2 \tag{11b}$$

and

$$F_{rs} = \mu N_s^2 J_s^2 (r_s/2R) \quad (12a)$$

$$F_{Rs} = - \mu N_s^2 J_s^2 (r_s/R)^2/4 - \mu N_p N_s J_p J_s r_p^2/2R^2 \quad (12b)$$

In the absence of stray inductances and resistances, and with no load in the secondary circuit, $M_{ps}J_p = - L_sJ_s$, so $N_sJ_s = - N_pJ_p (r_p/r_s)^2$. The force equations then simplify to:

$$F_{rp} = - \mu N_p^2 J_p^2 (r_p/R)[(r_p/r_s)^2 - 1/2] \quad (13a)$$

$$F_{Rp} = \mu N_p^2 J_p^2 (r_p/R)^2[(r_p/r_s)^2 - 1/2]/2 \quad (13b)$$

and

$$F_{rs} = \mu N_p^2 J_p^2 (r_s/2R)(r_p/r_s)^4 \quad (14a)$$

$$F_{Rs} = \mu N_p^2 J_p^2 (r_s/R)^2 (r_p/r_s)^4 /4 \quad (14b)$$

For $(r_p/r_s)^2 = k = 0.9$, the primary turns are under compression in the minor radius and pulling apart along their major circumference. The secondary circuit experiences tension along both the minor and major circumferential directions. Basically, for a well-coupled transformer (without complications of other inductances, resistances and secondary load), the magnetic field inside the primary is largely cancelled, leaving the magnetic field between the primary and secondary conductors. The magnetic pressure of this outer field presses the primary inward and the secondary outward. The "magnetic tension" is overcome by the magnetic pressure, so the secondary would attempt to expand its major radius. Interestingly, the primary turns would pull apart along their major radius.

The mechanical stresses opposing the movement of the conductors may be estimated from the preceding force equations, if we make some simplifying assumptions about the geometry. For example, by dividing Eqn. 14a by the surface area of the secondary, we obtain an equivalent pressure:

$$p_s = F_{rs}/(4\pi^2 R r_s) = \mu N_p^2 J_p^2 (r_p/r_s)^4/8\pi^2 R^2 \quad (15)$$

Note that the magnetic field associated with the secondary current is:

$$B_s = \mu N_p J_p (r_p/r_s)^2/2\pi R \quad (16)$$

so p_s is merely the magnetic pressure $B_s^2/2m$.

If we ignore the complex geometry of the toroid, in favor of the simpler situation of a thin-walled cylinder, the stress in the minor circumference is:

$$S_{rs} = p_s r_s/d_s = \mu N_p^2 J_p^2 (r_p/r_s)^4 (r_s/d_s)/8\pi^2 R^2 \quad (17)$$

The stress along the major circumference is similarly:

$$S_{Rs} = F_{Rs}/2\pi r_s d_s = \mu N_p^2 J_p^2 (r_s/R)^2 (r_p/r_s)^4/8\pi r_s \quad (18)$$

As a numerical example, suppose $N_p = 4$, $J_p = 3$ MA, $k = 0.9$, $R = 25$ cm, $r_s = 5$ cm, and $d_s = 1$ cm, the minor hoop stress is $S_{rs} = 21.8$ kpsi, while the major hoop stress is $S_{Rs} = 68.5$ kpsi. The former stress is about a factor of two below the yield strength of aluminum, so we may have an adequate solution, even with a static calculation; the latter stress suggests that (statically) we may have a problem. We still need to examine the situation for the actual waveforms from the time-dependent circuit calculation, using the earlier force formulas (Eqns. 11-12). Furthermore, we should integrate these forces over time to compute the impulses, which then permit calculation of the strains that might occur.

If we equate the kinetic energy associated with the impulse to the elastic strain energy, we may estimate the strains and associated stresses. For an impulse I shared by a mass M, the kinetic energy is:

$$W_K = I^2/2M \quad (19)$$

where I = Ft, based on the circuit calculations, and M = rAh for a cross-section A and a length h in the direction of the stress; this assumes that the impulse can indeed be shared with the full cross-section and length. The energy associated with simple elastic deformation is:

$$W_E = \int SAh\, de = EAh\, e^2/2 \quad (20)$$

where e is the strain and E is the elastic (Young's) modulus of the material. In terms of the stress S_m at the maximum strain:

$$W_E = S_m^2 Ah/2E \quad (21)$$

This stress is then related to the impulse by:

$$S_m = (E/r)^{1/2} I/Ah \quad (22)$$

As a numerical example, let's look at the stress in the major circumference of the secondary. For this, $A = 2pr_sd_s$, $h = 2\pi R$, and the impulse, based on Eqn. 14b, is:

$$I = \mu\tau\, N_p^2 J_p^2 (r_s/R)^2 (r_p/r_s)^4/4 \quad (23)$$

With values as before, and choosing an effective pulse time $\tau = 10$ μs, the impulse is I = 14.7 nt-s. For aluminum, with E = 10 Mpsi (= 6.8×10^{10} nt/m^2) and r = 2.7×10^3 kg/m^3, the peak stress is $S_m = 2190$ psi. This is considerably lower than the static value previously computed.

A separate concern is the combination of stresses on the primary coils. Around the major circumference, the individual coils will tend to move apart. They are wrapped,

however, in a way that will limit their basic azimuthal motion. It may nevertheless reduce frictional coupling between adjacent coils. The force in the minor radial direction is inward, so we may need to support the primary coils against such motion, perhaps with internal dielectric sections. Calculations based on impulse should indicate whether or not this will be necessary.

Finally, we must address the mechanical support of the disc transmission plates and their connections to the secondary. In addition to the usual forces driving the plates apart, we have the resultant forces needed to connect the hoop stress components in the minor circumference of the secondary. This hoop stress is "cut" by the exit gap needed to release magnetic energy to the liner load and must be replaced by some sort of clamping/buttress arrangement, operating across the secondary-side voltage difference. Such arrangements, of course, are needed for the disc plates as well. With the self-inductance of the disc transmission-plates:

$$L_{tp} = (\mu/2\pi)d \ln(r_{d2}/r_{d1}) \quad (24)$$

where r_{d2} is the plate radius near the connection to the secondary, r_{d1} is the radius of connection near the liner and d is the plate separation, the total force, attempting to push the plates apart is:

$$F_{tp} = (\mu/4\pi)\ln(r_{d2}/r_{d1})\, N_s^2 J_s^2 = (\mu/4\pi)\ln(r_{d2}/r_{d1})\, N_p^2 J_p^2 (r_p/r_s)^4 \quad (25)$$

As a numerical example, with $r_{d2}/r_{d1} = 10$ and other values as before, the required clamping force to hold the plates together statically is $F_{tp} = 26.9$ Mnt = 6 Mlbf. An estimate based on impulse requires a specification of the clamping arrangement and is deferred to later design.

Simplified modeling has been undertaken utilizing the RAVEN 1-D MHD code [5]. This modeling takes an expected driving current waveform ($T_{rise} \sim 2$ μs, $I_{max} \sim 5$ MA) and applies it to concentric cylindrical electrodes in a theta-pinch geometry. The electrode materials have tabular EOS and simple strength models incorporated into the hydrodynamics. The purpose here is to solve for the stresses in the outer electrode, compare to the theoretical prediction, and judge whether the electrode will survive repeated shots without encountering permanent damage due to plastic deformation.

In Fig. 10 the radial profiles of various quantities of interest are plotted at peak current. The material density (blue) is the nominal 2.7 g/cc of aluminum for an inner conductor (2 mm thick) and outer conductor (1 cm thick) with nominal 12 cm radius. The pressure generated (red) is a negligible fraction (<100 bar) of the nominal yield strength (2.6 kbar) of aluminum even with current densities of ($\sim 10^{10}$ A/m^2). From this analysis, it is expected multiple shots on the PHELIX transformer should not cause permanent damage.

For comparison, the formula for the stress on the secondary coil is evaluated. The parameters chosen are representative of the actual PHELIX transformer currently under construction. Here, $N_p = 4$, $N_s = 1$, $r_p = 11.4$ cm, $r_s = 12.0$ cm, $h = 2\pi \cdot 36$ cm = 226 cm, I = 5 MA. These give $S_{s,r} \sim 50$ bar and $S_{s,z} \sim 150$ bar. These are consistent with the results of the 1D modeling as well as much less than the nominal yield strength of aluminum.

To estimate electromagnetic forces in the transformer, an electromagnetic model of a single segment of the transformer was developed in ANSYS 12.0. The model is constructed using a parametric scripting file and three-dimensional electromagnetic brick and tetrahedral elements. The transformer's secondary side is a floating ground potential, while the primary coil within the transformer is pulsed with a varying AC current output from the RAVEN code. The current developed in the primary coil is used to solve for the magnetic field and forces in the secondary side of the transformer.

The PHELIX transformer is a symmetric toroidal transformer, which is split into 20 segments. Due to this segmented geometry, the model is made up of a single segment with periodic geometry boundary conditions at its radial faces. This resulted in a model made up of 5.8 million nodes, allowing excellent spatial resolution in the solved magnetic field and forces. Fig. 11(a) shows the mesh for 3D simulation. Fig. 11(b) shows a close-up of the meshing of the entrance/exit of the 2 helical coils. Fig. 11(c) shows the single-turn secondary coil colored by induced magnetic field. The green/yellow/red indicated that field only penetrates a small distance into the inner surface of the conductor as expected. Future work will include importing the magnetic nodal forces into a transient structural model to estimate mechanical stresses and life expectancies of the transformer's components.

IV. Summary

The Precision High-Energy density Liner Implosion eXperiment, PHELIX, is being designed and constructed at for use in conjunction with the LANL proton radiography diagnostics. It is aligned with the goals of the next-generation LANL signature facility, MaRIE. When operational, PHELIX will be capable of delivering 5-10 MA of peak current to a centimeter size liner load. Peak liner velocities will be in the range of 1-2 km/s. This driving capability can be used to place continuum size targets in the extreme conditions necessary to explore material science issues of dynamic spall.

PHELIX will be portable so that it can be taken to the diagnostic of choice. The high spatial resolution and high frame rate of the LANL proton radiography facility will reduce the number of shots in any particular experimental campaign, thus making PHELIX an economical platform for material science.

A theoretical analysis of the stresses on a pulsed high-current transformer is presented. Using an inductance

gradient method and a long-cylindrical, static approximation of a toroidal configuration, formula for both the radial and axial forces are found. For the primary coil, compressive forces are present in the radial direction for $r_p/r_s > ½$, while tensile forces are always present in the axial direction. For the secondary coil, tensile forces are always present in both the radial and axial directions. Using the formula for the forces on the secondary coil, the total stress was evaluated. It is shown to be comparable to 1D MHD simulations of concentric electrodes in in a θ-pinch configuration.

APPENDIX: ESTIMATE OF CRUSHING OF PRIMARY TURNS

In the same spirit as the earlier estimates of the stresses in the secondary, we may consider the effects of compression in the minor radial direction of the primary turns. This consideration is complicated by several factors, including the helical layout of the material (vs the simple cylindrical approximations for the secondary circuit) and the concentration of stress first in the conducting material (e.g., Cu), but partially supported by the larger diameter of insulation (with a much lower elastic modulus). The total force (for the shorted secondary example) is:

$$F_{rp} = - \mu N_p^2 J_p^2 (r_p/R)[(r_p/r_s)^2 - 1/2] \quad (26)$$

We may estimate an average equivalent pressure by dividing this by the surface area of the primary, $4\pi^2 r_p R$:

$$p = \mu N_p^2 J_p^2 (r_p/R)[(r_p/r_s)^2 - 1/2]/ 4\pi^2 r_p R \quad (27)$$

The stress in the primary (as compression in the minor hoop direction) may then be written as:

$$S_{hp} = p(r_p/d_p) f_{cp} \quad (28)$$

where d_p is the thickness of the primary turn and f_{cp} is a concentration factor for the uniformly applied stress compared to the discrete size of the turns:

$$f_{cp} = 2\pi R d_p/N_p N_c(\pi d_p^2/4) \quad (29)$$

with N_c the number of cables that are used to assemble the primary. Substitution provides:

$$S_{hp} = 2\mu N_p J_p^2 (r_p/R)[(r_p/r_s)^2 - 1/2] /N_c \pi^2 d_p^2 \quad (30)$$

Based on the same values previously employed, and with $N_c = 48$, we have:

$$S_{hp} = 2.13 \times 10^6 \text{ [psi]}/ d_p^2[\text{mm}^2] \quad (31)$$

For a center conductor diameter of 0.115" (2.92 mm), the stress in the copper (unsupported by the surrounding plastic) is about 250 kpsi, so the copper would yield, if this were a static load. If we ignore the copper and use only the insulator, with a diameter of 0.375" (9.53 mm), the stress is reduced to 23.5 kpsi, which is more than the plastic would allow statically.

To consider the effects of the short pulse duration, we return to the impulse formulation, writing here the kinetic energy provided to a single turn in time τ as:

$$w_K = (S_{hp} A\tau)^2/2r(2\pi r_p A) = S_{hp}^2 A\tau^2/4\pi r_p r \quad (32)$$

where $A = \pi d_p^2/4$ is the cross-sectional area of the turn. The elastic energy is:

$$w_E = S_m^2 (2\pi r_p A)/2E \quad (33)$$

so the maximum stress obtained by equating the kinetic and elastic energies is:

$$S_m = S_{hp} (E/r)^{1/2} \tau/2\pi r_p \quad (34)$$

For plastic, with E = 100 kpsi and r = 1.2 g/cm^3, the elastic speed is $(E/r)^{1/2}$ = 753 m/s. With r_p = 4.74 cm and τ = 10 μs again, the maximum stress would be S_m = 594 psi. If we apply the same factor to reduce the stress in unsupported copper, the stress would become 6.3 kpsi. These impulsive stress values are not too far away from the yield strengths of plastic and copper, respectively, so more detailed calculations (e.g., including the actual current waveforms) are warranted.

REFERENCES

[1] "MaRIE to Become LANL's Signature Experimental Facility," LALP-09-035, 14 (2009).

[2] C. Morris, J. W. Hopson, P. Goldstone, "Proton Radiography," *Los Alamos Science*, No. 30, pg 32 (2006).

[3] P. J. Turchi, "Scaling of Pulsed Power-Driven Hydrodynamics Experiments with Capacitors and Flux-Compressors," IEEE Trans. on Plasma Science, 34, 5, 1919 (2006).

[4] P. J. Turchi, W.L. Atchison, J. R. Griego, W. A. Reass, R. E. Reinovsky, C. L. Rousculp, "PHELIX: Design of Transformer-Driven Liner Implosion System," in *Proc. of 12th Intern. Conf. on Megagauss Magnetic Field Generation and Related Topics*, Novosibirsk, 13 – 18 July 2008. G.A. Shvetsov, ed.

[5] T. A. Oliphant and K. H. Witte, RAVEN, LA-10826, 1987.

[6] P. J. Turchi, "Electric Rocket Propulsion Systems", in Space Propulsion Analysis and Design, R. Humble, G. Henry and W. Larson, eds., McGraw-Hill (1995). Chapter 9.

Fig. 1 Sequence of proton radiographs of dynamic spall with time running from top to bottom.

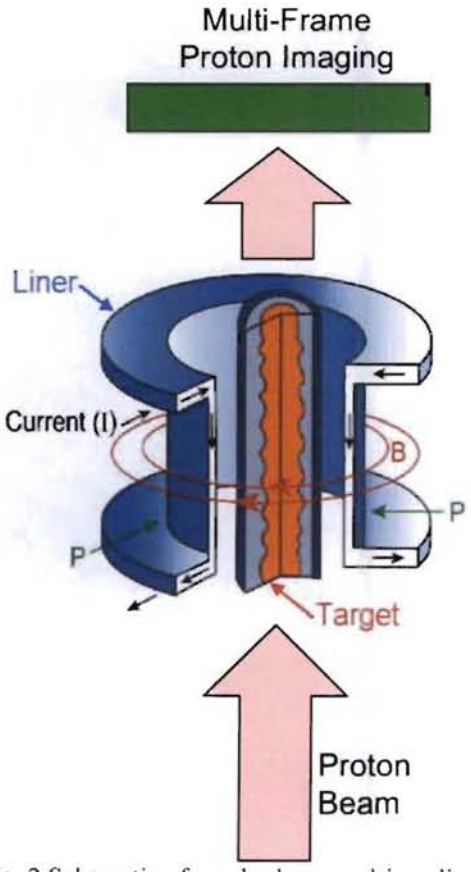

Fig. 2 Schematic of a pulsed power driven liner on target experiment utilizing proton radiography as an axial diagnostic.

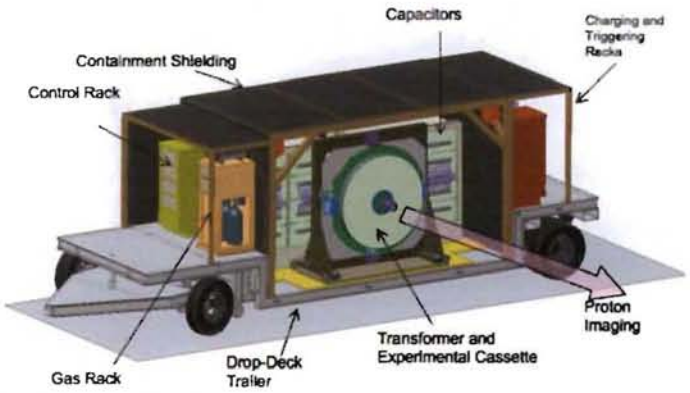

Fig. 3 The PHELIX portable pulsed power machine.

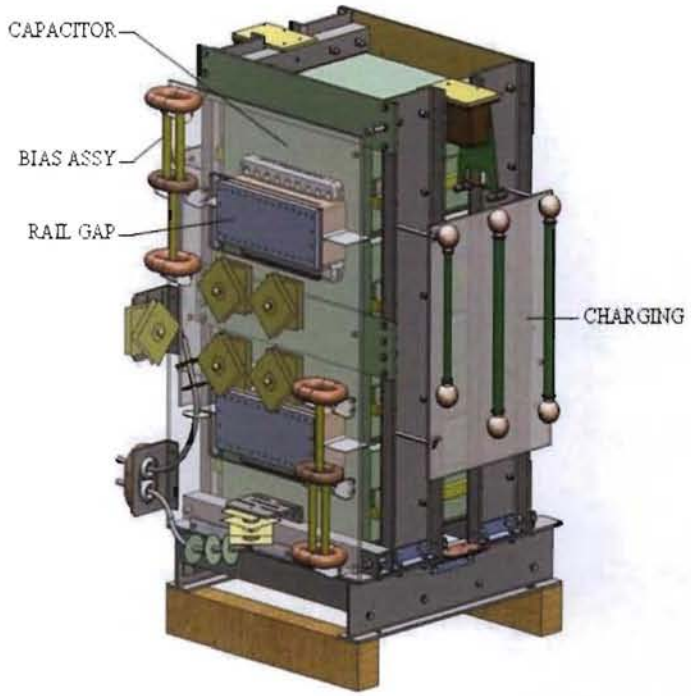

Fig. 4 Fiberglass air insulated marx support structure with fiberglass capacitors, railgaps, charging, and trigger bias assemblies.

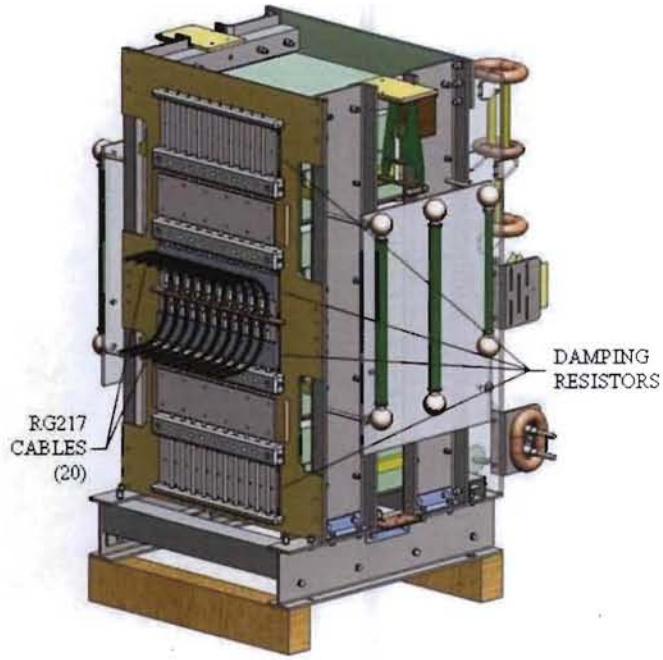

Fig. 5 Marx output header assembly with damping resistors and cables

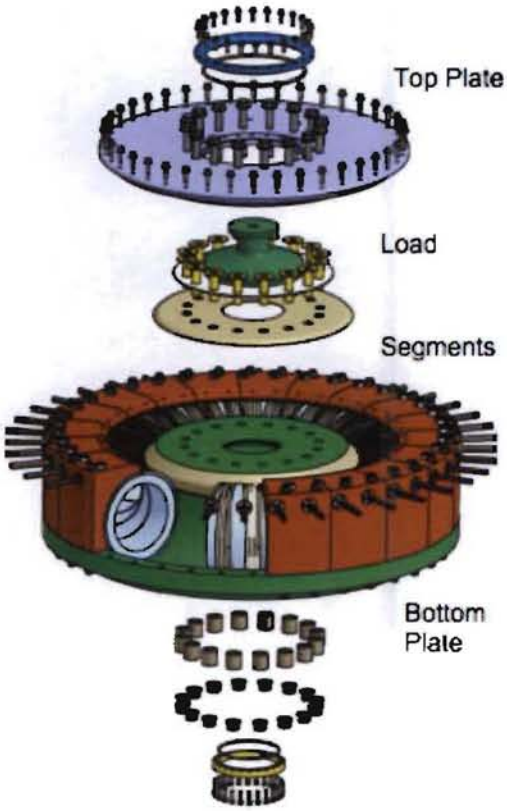

Fig. 6 Exploded view of the PHELIX transformer.

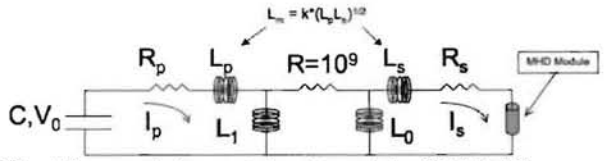

Fig. 7 Lumped element circuit model of PHELIX.

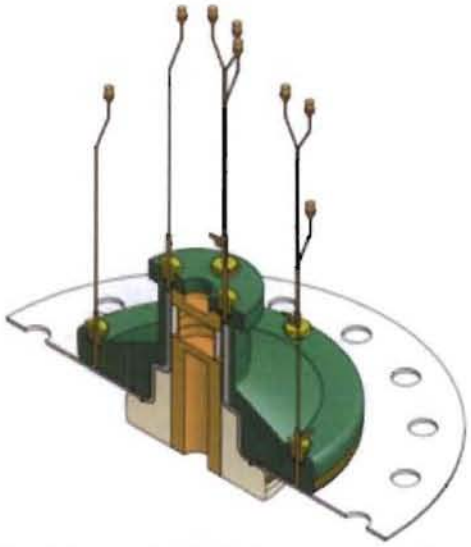

Fig. 8 Simple PHELIX liner cassette with several leads for b-dot probe diagnostics.

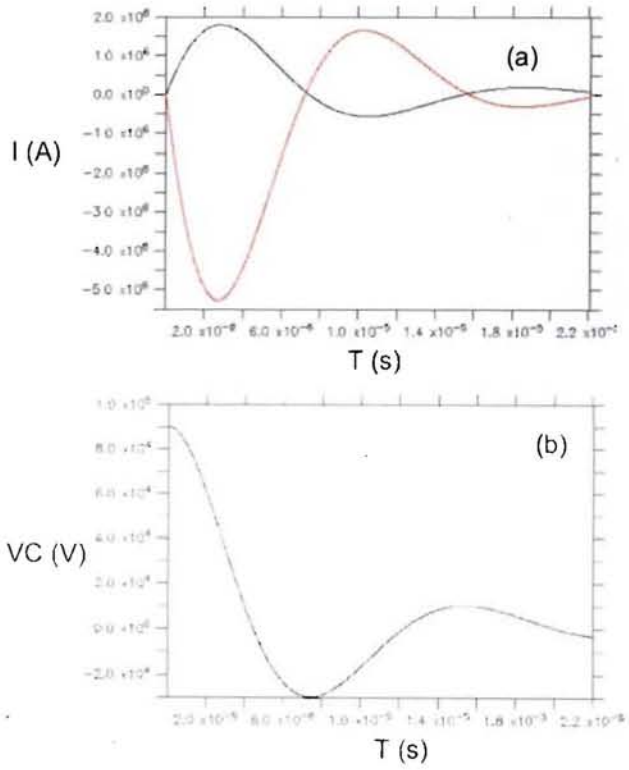

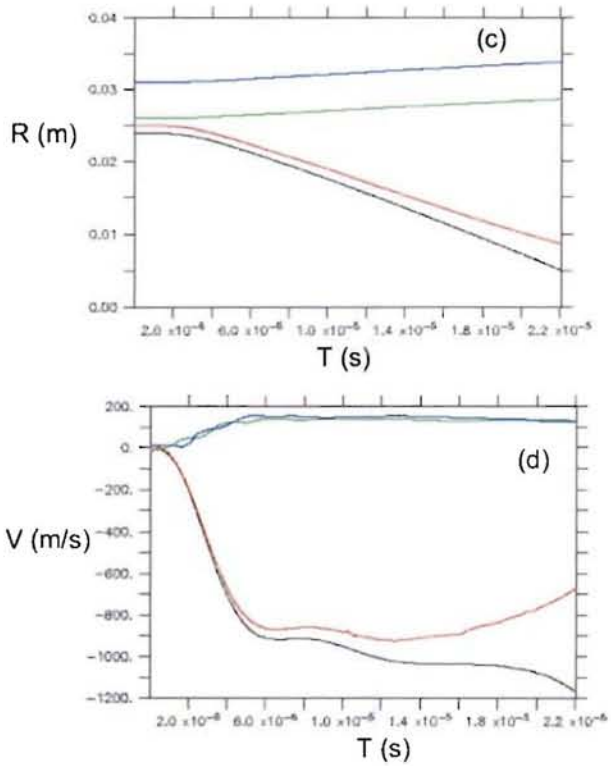

Fig. 9 Solution for coupled PHELIX circuit and MHD of a simple liner: (a) Transformer primary (black) and secondary (red) currents, (b) capacitor voltage, (c) liner (red/black) and return conductor (blue/green) surface trajectories, (d) liner (red/black) and return conductor (blue/green) surface velocities.

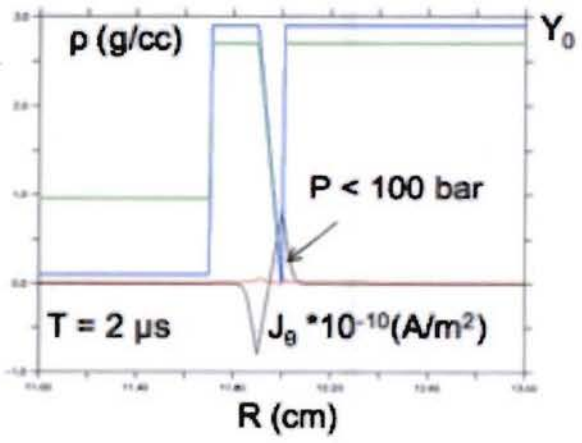

Fig. 10 Radial profiles of current density (black), material density (green), pressure (red), and yield strength (blue) of 2 concentric electrodes subject to a θ-directed current.

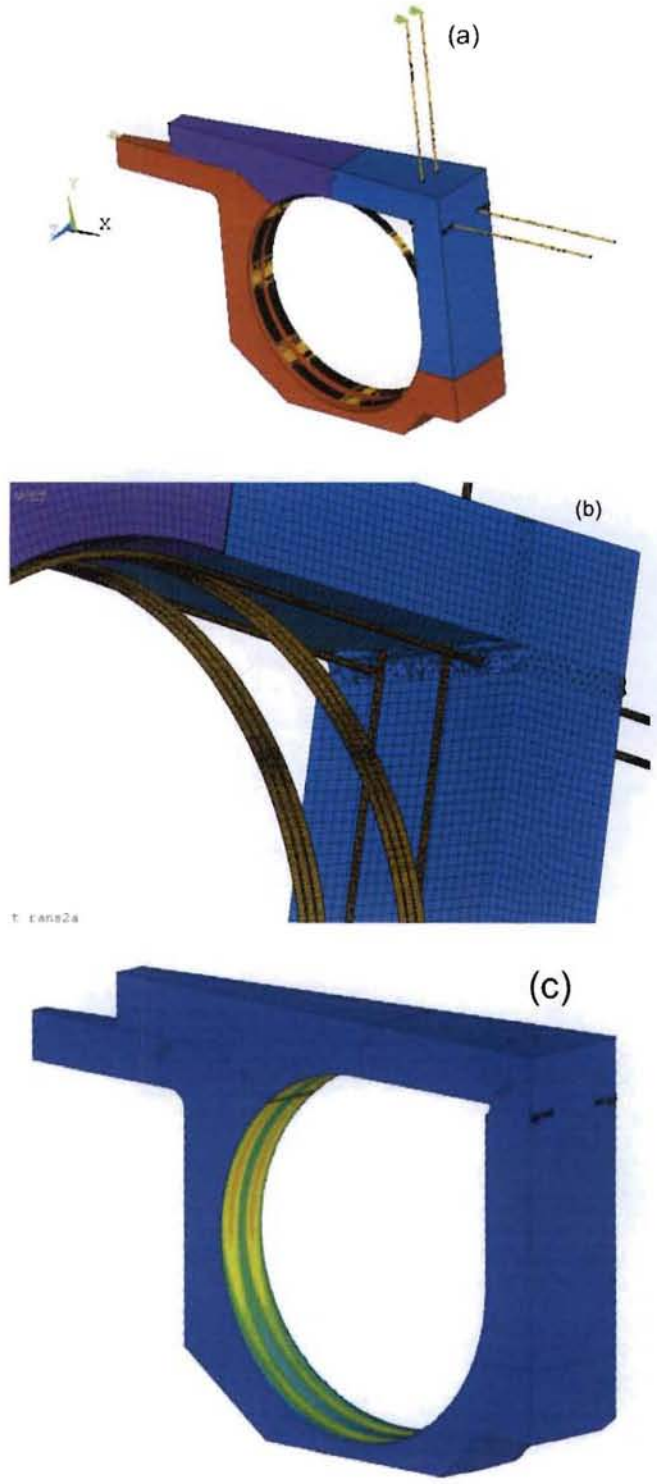

Fig. 11 (a) 5.8 million element, 3D model of a single segment of the PHELIX toroidal transformer. (b) Close-up of the meshing of the entrance/exit of the helical coils from the transformer segment. (c) Single-turn secondary coil colored by the induced magnetic field.